Growth and magnetic properties of iron-based oxide thin films deposited by pulsed laser deposition at room temperature

X. Portier, E. Millon, V. Demange, S. Ollivier, M. Guilloux-Viry, M. Nistor, C. Hebert, C. Cachoncinlle, J. Perrière

Growth and magnetic properties of iron-based oxide thin films deposited by pulsed-laser deposition at room temperature

X. Portier[1], E. Millon[2*], V. Demange[3], S. Ollivier[3], M. Guilloux-Viry[3], M. Nistor[4], C. Hebert[5], C. Cachoncinlle[2], J. Perrière[5]

[1] Centre de recherche sur les Ions, les MAtériaux et la Photonique (CIMAP), CEA, UMR CNRS 6252, Normandie Université, ENSICAEN, 14050 Caen Cedex, France

[2] Groupe de Recherche sur les Milieux Ionisés (GREMI), UMR 7344 CNRS - Université d'Orléans, 45067 Orléans Cedex 2, France

[3] Institut des Sciences Chimiques de Rennes (ISCR), UMR 6226 CNRS - Université de Rennes, ScanMAT – UAR 2025, 35000 Rennes, France

[4] National Institute for Lasers, Plasma and Radiation Physics (NILPRP), PO Box MG-36, 077125 Magurele-Bucharest, Romania

[5] Institut des NanoSciences de Paris (INSP), UMR 7588 CNRS - Sorbonne Université, 4 Place Jussieu, 75252 Paris Cedex 05, France

***** : corresponding author : eric.millon@univ-orleans.fr

Abstract

In the present work, room temperature epitaxial growth of Zn-doped iron oxide films (Zn:FeO_x) was achieved by pulsed-laser deposition, on c-cut sapphire substrates without any high temperature thermal treatments before the growth. Rutherford backscattering spectrometry, atomic force microscopy, transmission electron microscopy, X-ray diffraction and pole figure measurements were used to determine the texture and in-plane epitaxial relationships between the films and the substrate. The nature of the oxide phases (wüstite and/or spinel) present in the films depends on the oxygen pressure during the laser ablation. At the residual vacuum ($2x10^{-7}$ mbar), the (111) wüstite (Zn:FeO) textures were obtained in the films, while oxygen pressures between $2x10^{-5}$ to $2x10^{-3}$ mbar led to the epitaxial growth of the spinel (Zn:Fe_3O_4) phase on the c-cut sapphire substrate. Magnetic properties through M(H) curves at 10K and 300K, of the wüstite-based film grown under $2x10^{-7}$ mbar were studied, and an exchange bias due to the presence of Fe^{3+} cation in the film is observed. Finally, the possible mechanisms of the room temperature epitaxial growth of the oxide films on the substrate are presented and discussed.

Keywords :

pulsed-laser deposition, Zn-doped iron oxide, thin film, epitaxy, magnetic properties

Introduction

The epitaxial growth of thin films on single crystalline substrates requires high temperatures (generally between 400°C and 600°C) [1-4]. However, epitaxial growth at lower temperatures presents some interesting features such as (i) to avoid the interdiffusion reaction of species between the film and the substrate, (ii) to avoid defects formation, such as cracks, resulting from difference in thermal coefficients of the film and of the substrate and (iii) to reduce the manufacturing cost by lowering the thermal budget during the fabrication of application-relevant devices [5]. It has been shown that Ni-Zn ferrite, Mn-Zn ferrite and ZnO epitaxial films can be grown at low temperatures [6, 7], and that a wide variety of epitaxial films of oxides and nitrides were obtained at room temperature (RT) with different textures on various substrates such as Si [8], $SrTiO_3$ [9], $LaAlO_3$ [10], ZnO [11]. Most of these studies have been achieved using the pulsed-laser deposition (PLD) technique and the pre-annealed (001) oriented sapphire (c-cut) as substrate [12-16]. The c-cut sapphire substrate pre-annealed in ambient air at high temperature (1000°C), presents steps and terraces on the (001) plane, which play the role of nucleation centers for the epitaxial growth [17, 18]. Additionally, with PLD, the species emitted by the target during laser ablation exhibit a high kinetic energy up to tens eV [19], which allows them to have a high surface mobility at RT leading to the crystallization of the film on the substrate [20, 21].

Iron-oxide films based on wüstite (FeO) or magnetite (Fe_3O_4) phases are interesting due to their magnetic properties [22, 23]. Such films can be grown by PLD and it has been demonstrated that iron oxide films can be epitaxied onto single crystal substrates. Indeed, Fe_3O_4 films can be easily obtained by PLD on various single crystal substrates such Si (111), GaAs (100) or Al_2O_3 c-cut sapphire (001) held at 450°C [24]: in the case of c-cut sapphire substrate, the magnetite films are found to be oriented along the [111] direction. On the contrary, the growth of a single-phase wüstite film is more challenging as FeO is thermodynamically stable above 575°C at atmospheric pressure making the growth at RT of wüstite films free of magnetite difficult to achieve. As a result, it has been evidenced that Fe_3O_4 films can be obtained at RT by laser molecular beam epitaxy [25]. In the same way, a mixture of Fe_3O_4 and FeO based films have been grown by PLD on c-cut sapphire substrate at RT [26]. One way to make the growth of wüstite films possible at RT is a partial substitution of iron by zinc to obtain a solid solution Zn-doped wüstite. Recently, Zn-doped iron oxide films have been obtained at RT on a-cut ((110) oriented) and r-cut ((102) oriented) sapphire substrate by pulsed-laser ablation of a Zn:Fe_3O_4 ($Zn_{0.85}Fe_{2.15}O_4$) target under a $7x10^{-6}$ mbar oxygen residual pressure [27]. In [27], the epitaxial relationships between the Zn-doped iron oxide (labelled ZFO) films and the sapphire substrates have been evidenced. Despite the low partial pressure used ($7x10^{-6}$ mbar), the ZFO films showed the presence of the Zn-doped wüstite phase only located at the bottom of the film (the 15st nm near the interface with the substrate) while the remaining upper part of the films is constituted by the spinel phase. Following this way, the oxygen partial pressure is a key parameter to preferentially grow wüstite-based ZFO film at RT.

In the present work, we aim to study the RT epitaxial growth of Zn-doped iron oxide (Zn:FeO_x; ZFO) on c-cut sapphire substrates using different oxygen partial pressures ($2x10^{-7}$ mbar, $2x10^{-5}$ mbar and $2x10^{-3}$ mbar) and a target containing around 25%at. of Zn. In particular, the very low partial pressure of $2x10^{-7}$ mbar is expected to favor the growth of the Zn-doped wüstite phase Zn:FeO (denoted ZFO_W in the following). The c-cut sapphire substrates were not pre-annealed before the film growth to prevent the formation of nucleation centers for the growth [17, 18]. The epitaxial relationships between these phases and the (001) Al_2O_3 plane were deduced from X-ray diffraction (XRD) and transmission electron microscopy (TEM) experiments. We show that a nearly pure Zn-doped wüstite phase is grown under $2x10^{-7}$ mbar

(vacuum limit). At higher pressures ($2x10^{-5}$ and $2x10^{-3}$ mbar), the ZFO films are constituted with the Zn-doped magnetite phase $Zn:Fe_3O_4$ (denoted ZFO_S). Magnetic measurements through M(H) curves at 10K and 300K of the wüstite-based film grown under $2x10^{-7}$ mbar, show the coexistence of ferromagnet-antiferromagnet interactions that confirms the presence of Fe^{3+} cations evidenced by electron energy loss spectrometry (EELS).

Experimental

The Zn-doped iron oxide films were obtained by PLD [28-30] using a frequency - quadrupled Nd:YAG laser (λ = 266 nm, τ = 7 ns, 10 Hz repetition rate) in the experimental device already described elsewhere [31]. A $Zn:Fe_3O_4$ ceramic target (Zn concentration equal to about 25%at.) was irradiated with laser pulses that leads to a laser fluence of 2 J/cm^2. As the crystalline structure and the properties of the oxide films are depending on their oxygen composition [32-35], the growth was carried out under 3 different oxygen pressures : $2x10^{-7}$ mbar (residual vacuum), $2x10^{-5}$ mbar and $2x10^{-3}$ mbar. The raw c-cut sapphire substrates supplied by Crystec GmbH were held at RT without any high temperature thermal treatment before the PLD growth.

Atomic force microscopy (AFM) images, using an AFM NT-MDT Ntegra instrument, were recorded to study the surface topography of the bare substrates before the growth and of the obtained film.

The film thickness (in the 60 to 100 nm range) and in-depth distribution of the elements were quantitatively obtained by Rutherford backscattering spectroscopy (RBS) using the 2.5 MeV ion beam from the van de Graaff accelerator (SAFIR) of INSP (Sorbonne Université). The respective Zn and Fe concentrations in the films were determined from the simulation of the RBS spectra with the RUMP program, with a 1% accuracy, while the oxygen content was only obtained with a 4% precision. The O/Fe ratio which is related to the obtained Fe-O phases (i.e. wüstite, and magnetite spinel) in the films, and the Zn/Fe+Zn ratio related to the Zn doping in the ZFO films can be deduced from these experiments.

XRD analyses were performed on a Bruker D8 Advance diffractometer and on a XPert Panalytical 4 circles diffractometer. XRD was used to determine the nature of the phases present in the films and their texture. The epitaxial relationships between film and substrate were deduced from asymmetric diffraction, i.e. phi scan and/or pole figure measurements.

Thin electron transparent cross-section foils for transmission electron microscopy observations were thinned down by a focused ion beam (FIB) equipment (Dual-beam FEI Helios nanolab 660). A carbon film (about 20 nm thick) and a Pt layer (a few microns thick) were deposited prior to the thinning process to protect the film from the gallium beam. The carbon film was introduced to discriminate the top surface of the film and the Pt protecting layer. TEM observations were performed with a double corrected cold FEG JEOL ARM 200F microscope, operated at 200 kV. Attached to the microscope was a post column GATAN QUANTUM ER electron energy loss spectrometer (EELS). This microscope had also a scanning setup (STEM mode with dark and bright field detectors) allowing the electron beam to be monitored with a spatial resolution of about 0.78 Å. All together, STEM EELS experiments were then possible in order to obtain EELS spectra, EELS profiles or even EELS mapping for a nanoscale region. All digitized images and EELS spectra were processed using the GMS2 Digitalmicrograph software from GATAN.

Finally, the magnetic properties were evaluated at 10K and 300K by the measurements of the magnetization M as a function of the applied magnetic applied field $\mu_0 H$ in the plane of the films.

Results

Chemical composition, phase identification and structural properties

AFM measurements have been carried out on the substrates and on the films (Fig. 1).

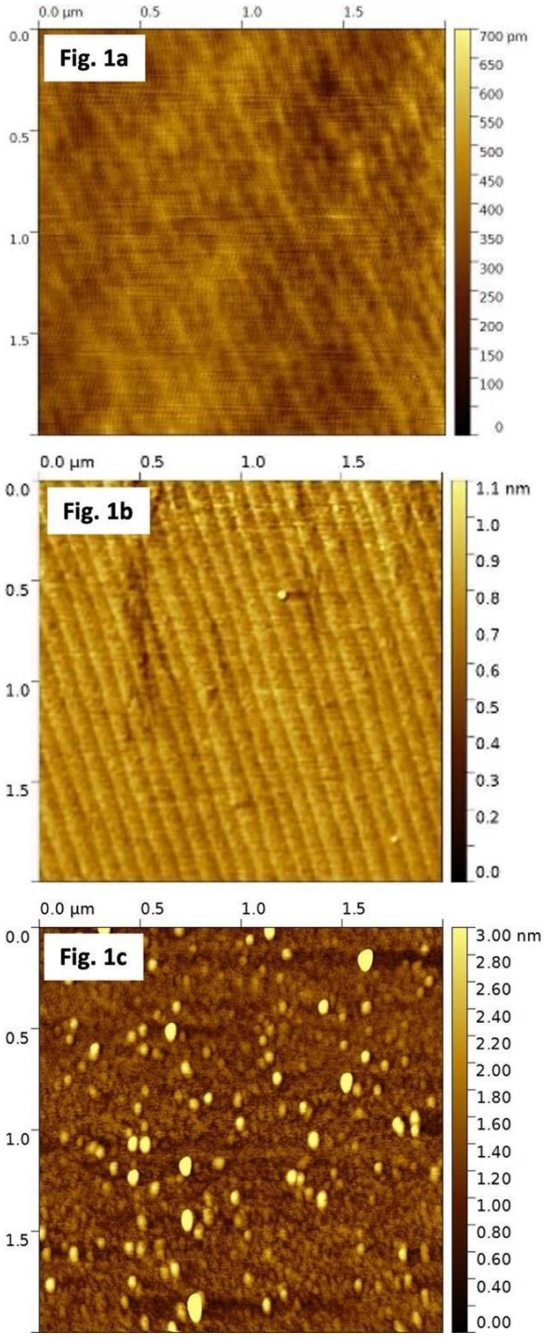

Fig. 1: AFM Images of a) a c-cut sapphire substrate as supplied by Crystec GmbH; b) a c-cut sapphire substrate pre-annealed for 2 hours at 1000°C in air; c) a ZFO film grown at RT under $2x10^{-7}$ mbar on a non pre-annealed c-cut sapphire substrate.

Fig. 1a shows an AFM image of a c-cut sapphire substrate as supplied by Crystek GmbH. The substrate has not been pre-annealed, and despite this fact, the presence of atomic steps and terraces can be distinguished on the surface. Such a surface morphology could be due to a slight miscut of the substrate. For comparison, Fig. 1b shows the AFM image of a c-cut sapphire substrate after thermal treatment in air (2 hours at 1000°C). In this image, the atomic steps and terraces are much more defined and regular than in Fig. 1a. Typically, the atomic step height is about 0.2 nm, and terraces about 100 nm width can be obtained at 1000°C [25, 36]. In Fig. 1c, we present the AFM image of a ZFO film grown under $2x10^{-7}$ mbar at RT on a non pre-annealed c-cut sapphire substrate. The film surface appears to be formed by grains of different sizes, and the slight steps and terraces observed in Fig.1a, do not appear. It is noticed that for oxide films grown on c-cut substrates pre-annealed at 1000°C, a smooth surface with step and terraces is usually observed [25, 36], indicating that the growth at RT on such a substrate leads to the suppression of 3D grain growth.

Different phases are likely to be observed in a Zn-doped iron oxide material, namely wüstite (ZFO_W) with the rocksalt structure, magnetite (ZFO_S) with the spinel structure and hematite ($Zn:Fe_2O_3$ denoted ZFO_H). The oxygen/iron ratio in these phases is different and a low oxygen composition in the film will favor the formation of the wüstite phase. Increasing the oxygen composition will lead to the magnetite spinel phase, and a further increase will give rise to the hematite phase. As the aim of our study is particularly focused on the growth of the metastable wüstite phase at RT, the experiments were carried out at low oxygen pressure. As a result, the PLD growth at RT was performed for three oxygen pressures: $2x10^{-7}$ (vacuum limit), $2x10^{-5}$ and $2x10^{-3}$ mbar oxygen pressures. Above $2x10^{-3}$ mbar, the ZFO films are amorphous with a composition corresponding to the hematite phase (O/(Fe+Zn) ratio around 1.5).

RBS was used to determine the composition of the ZFO films grown at RT for the different oxygen pressures. The spectra obtained (not shown here) do not evidence the presence of impurities in the films or interdiffusion between the film and the substrate. The distribution of the elements Fe, Zn and O is homogeneous throughout the thickness of the film (ranging from about 60 to 100 nm depending on the oxygen pressure). The composition of the three ZFO films deduced from the RBS spectra are summarized in Table I.

Pressure (mbar)	Composition (RBS)	Zn/(Fe+Zn)	O/(Fe+Zn)	O/Fe	Film thickness (nm)	Phase (XRD)	*hkl*: 2θ	Lattice parameter *a* (nm)
$2x10^{-3}$	$Zn_{0.68}Fe_{2.28}O_4$ $0.68(ZnO)0.83(Fe_{2.75}O_4)$	0.23	1.35	1.45	66	$Zn:Fe_3O_4$	111: 18.08° 222: 36.61°	0.849 +/- 0.002
$2x10^{-5}$	$Zn_{0.75}Fe_{2.39}O_4$ $0.75(ZnO)0.81(Fe_{2.95}O_4)$	0.24	1.27	1.35	94	$Zn:Fe_3O_4$	111: 18.09° 222: 36.64°	0.848 +/- 0.002
$2x10^{-7}$	$Zn_{0.21}Fe_{0.67}O_1$ $0.21(ZnO)0.79(Fe_{0.85}O_1)$	0.24	1.13	1.17	84	Zn:FeO	111: 36.07°	0.430 +/- 0.002

Table I : Chemical composition deduced from RBS analyses, nature of phases and crystallographic cell parameter obtained from XRD measurements for the films grown at RT under different oxygen pressures.

The atomic ratios given in Table I, show that the concentration of Zn in the films is around 23-24% and is not significantly affected by the oxygen partial pressure. On the contrary, the O/ (Fe+Zn) ratios decrease following the oxygen pressure. According to these ratios, the chemical formulas are presented with stoichiometric coefficients corresponding to the expected crystallographic phases, i.e. ZFO_S (spinel structure) and ZFO_W (wüstite structure) as observed in the following. In addition, the theoretical formulas expressed as "a(ZnO)b($Fe_{3-x}O_4$)" or "a(ZnO)b($Fe_{1-x}O$)" given in Table I, are based on the fact that O^{2-} anions are linked in one hand to Zn^{2+} and in the other hand to the Fe^{2+} and Fe^{3+} cations. Therefore, this makes it possible to estimate the O/Fe atomic ratio and consequently the effect of oxygen pressure on the formation of different iron oxide phases that will be discussed in more detail at a later stage in the paper.

To determine the nature of the phases present in the films, XRD measurements were carried out in the θ/2θ Bragg Brentano geometry. The diagrams of the ZFO films grown under the different oxygen pressures are displayed in Fig. 2 in the 15°to 40° 2θ range.

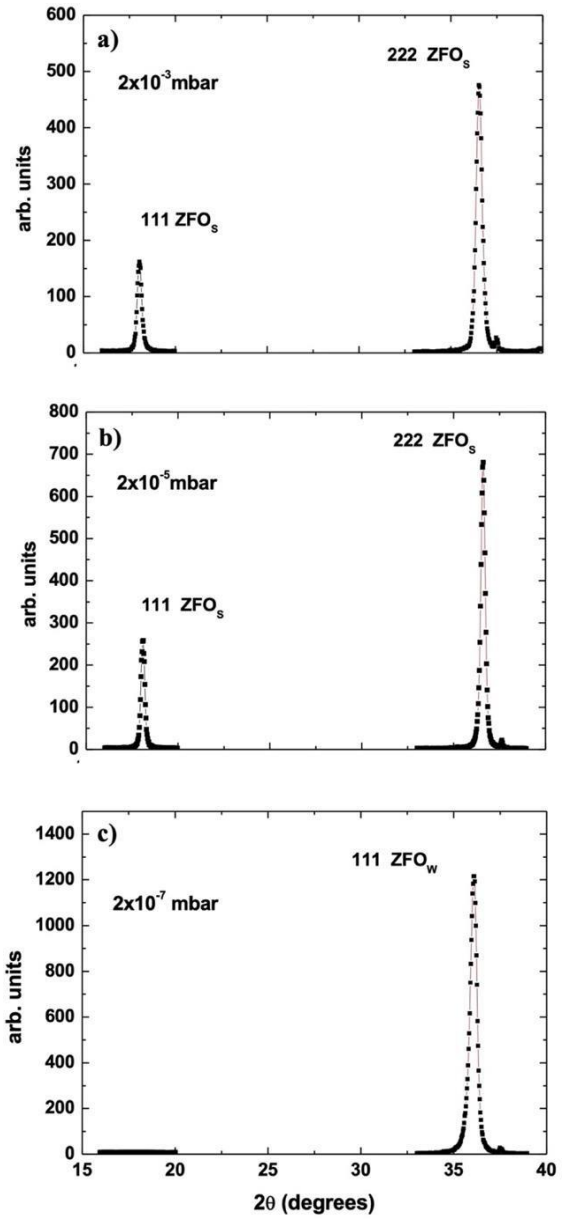

Fig. 2: θ/2θ XRD patterns of the three ZFO films grown at RT under a) $2x10^{-3}$, b) $2x10^{-5}$ and c) $2x10^{-7}$ mbar

The XRD patterns of the films show peaks related to the ZFO phase and a very weak diffraction line at around 2θ=37.4° corresponding to the (006) Al_2O_3 plane diffracted by the residual K_β line of the Cu radiation. No other phases (i.e. ZnO, Fe_2O_3...) are detected from these experiments. The film grown at high pressure ($2x10^{-3}$ mbar) shows the characteristic reflection peaks of the magnetite spinel ZFO_s phase following the (111) and (222) planes, at 2θ = 18.08° and 36.61° (Figs. 2a, Table I), respectively. At intermediate pressure ($2x10^{-5}$ mbar), the angular positions of these two peaks are 18.09° and 36.64° (Fig. 2b, Table I) On the contrary, the film grown under $2x10^{-7}$ mbar only shows a single peak at 36.07° which is attributed to the 111 reflection of the ZFO_w phase, while the 111 peak at around 18° is not present (Fig. 2c). The 2θ values of the (111) wüstite, (111) magnetite and (222) magnetite planes agree with FeO (ICDD #00-006-0615, *Fm*-3*m* space group, *a*=0.4307 nm) and Fe_3O_4 (ICDD #00-89-4319, *Fd*-3*m* space group, *a*=0.8395 nm) respectively, considering the variation of the lattice parameters due to Zn incorporation. As expected, a high oxygen pressure (at $2x10^{-5}$ mbar and above) leads to the growth of a magnetite spinel-based film. The use of vacuum limit (residual vacuum) condition makes it therefore possible to obtain at RT a crystallized ZFO film consisting of the wüstite phase, the magnetite phase not being detected by XRD measurements.

The lattice parameters *a* were calculated from the peak positions of the (*hhh*) family planes of the wüstite and spinel phases. The obtained values are given in Table I. Concerning the ZFO film grown at the highest pressures ($2x10^{-5}$ and $2x10^{-3}$ mbar), the lattice parameter *a* of the spinel phase is around 0.848-0.849 nm, a higher value than that of the undoped Fe_3O_4 phase (0.839 nm) or of $(Zn,Fe)_3O_4$ [37]. The *a* value deduced from the XRD peak position of the (111) and (222) magnetite planes in our film corresponds to a lattice distance parallel to the sapphire basal plane. The ZFO_s being oriented along the [111] direction, a difference between the [100] and [001] ZFO_s lattice parameters may not be excluded. Indeed, it has been shown that structural defects such as anti-phase boundaries, which separate two domains in the same phase, can occur in epitaxial Fe_3O_4 thin films grown on various single-crystal substrates (MgO, Al_2O_3...) [38]. This is the result of symmetry breaking during the growth and leads to the stacking of defects at the grain boundaries. As a result, differences between in-plane and out-of plane lattice parameters can be observed as a strong deviation of the out of plane lattice parameter referring to the *a* value of polycrystalline Fe_3O_4 [38].

Concerning the Zn-doped wüstite film grown under $2x10^{-7}$ mbar, the lattice parameter of the ZFO_w phase deduced from the XRD (111) peak position is very close (0.430 nm) to that of the stoichiometric FeO phase referenced in #00-006-0615 ICCD file (0.4307 nm). Before discussing this experimental value, it has to be reminded that the *a* value in such ZFO_w phase depends on the Zn dopant content and also on the concentration of Fe^{3+} and cationic vacancies. Considering first a stoichiometric wustite phase FeO (with O/Fe=1), the substitution of Fe^{2+} by Zn^{2+} following the Zn doping should induce a reduction in the unit cell volume as observed for ZFO_S since the ionic radius of Zn^{2+} (0.074 nm) is smaller than that of Fe^{2+} (0.076 nm). But in our case, the wüstite phase in the ZFO_w films is not stoichiometric (O/Fe>1). For an O/Fe ratio equal to 1.17 corresponding to the composition of our thin film, the formula can be written as $Fe_{0.855}O$, leading to concentrations of cationic vacancies and Fe^{3+} ions around 14.5% and 29%, respectively. In the case of an undoped $Fe_{1-x}O$ wüstite phase, such a presence of cationic vacancies results in a smaller lattice parameter "*a*". But as detailed in ref [39], the occupation with Zn^{2+} ions in the wüstite network can induce an increase of the lattice parameter following a charge balance effect with Fe^{3+}. According to this mechanism and considering the stoichiometric wüstite FeO (ICDD # 00-006-0615; *a*=0.4307 nm) as a reference, the lattice parameter in the non-stoichiometric wüstite $Fe_{0.855}O$ should be less than 0.4307 nm due to the formation of cationic vacancies and Fe^{3+} ions. The incorporation of Zn into $Fe_{0.855}O$ which

induces an increase of "a" [39], leads to finding a lattice parameter value (0.431 nm) for the ZFO film, very similar to a stoichiometric FeO wüstite.

The possible epitaxial relationships between the film and the c-cut sapphire substrate were first investigated by pole figure measurements using asymmetric XRD. For the films grown at $2x10^{-5}$ mbar and $2x10^{-3}$ mbar, and constituted with the magnetite spinel phase, the obtained epitaxial relationships have already been observed on similar samples in a previous studies and published in [24, 26, 40]. These are reminded below:

$$[10\text{-}1]\ ZFO_s\ //\ [210]\ Al_2O_3$$

This relationship corresponds to a 30° rotation of the hexagons of the magnetite spinel (111) plane with respect to the hexagons of the (001) sapphire. This was explained following the domain matching epitaxy (DME) through the relation $m\ d_{ZFOw} \approx p\ d_{Al2O3}$ [41-44] with the m = 7, and p = 5 which leads to a lattice mismatch $\delta = 0.9\%$ and a size of epitaxial domain of 4.2 nm [40].

Figure 3 shows the pole figure of the wüstite based-film grown at $2x10^{-7}$ mbar which was recorded for the (200) wüstite reflection at $2\theta = 42.2°$.

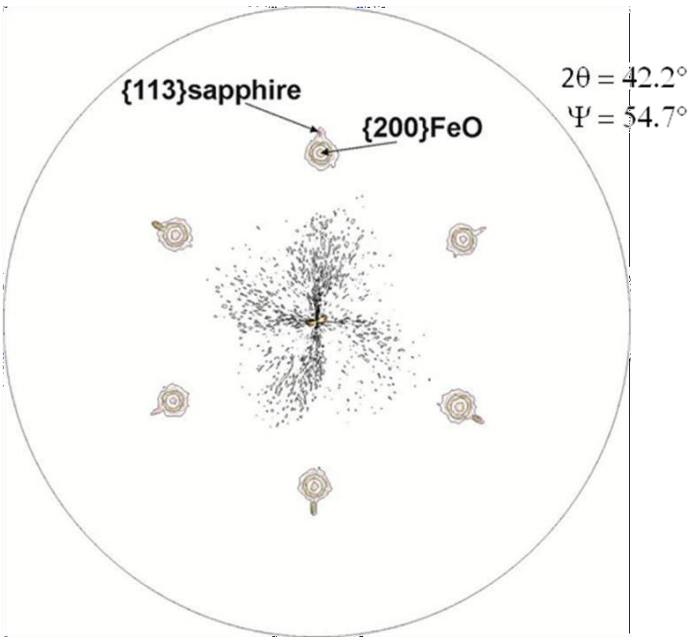

Fig. 3: XRD pole figure recorded on the 200 FeO reflections at $2\theta = 42.2°$ for the wüstite-based ZFO films grown at RT under $2x10^{-7}$ mbar. 113 sapphire reflections are also observed in the pole figure.

It shows six well-defined poles at a declination angle $\psi = 54.7°$, characteristic of the epitaxy of the wüstite phase. This pole figure characterizes again a 30° rotation of the hexagon of the (111) wüstite with respect to the hexagons of the (001) sapphire plane. The corresponding in-plane relationship is therefore as follows:

$$[10\text{-}1]\ ZFO_w\ //\ [210]\ Al_2O_3$$

The comparison of the respective interatomic distance of the substrate and of the film in the interface plane indicates that a lattice mismatch exists. Following the way involved for the wüstite based- ZFO film, the epitaxy is explained in the frame of DME. In this case, the

values m and p, given by the relation $m\ d_{ZFOw} \approx p\ d_{Al2O3}$, are m = 4 and p = 3 which leads to a lattice mismatch of δ = 1.6%, and a size of epitaxial domain of 1.2 nm.

The microstructure of the ZFO film at the atomic scale was also investigated by TEM analysis. Figure 4 shows cross sectional bright-field TEM images of the films grown at oxygen partial pressures of $2x10^{-3}$ mbar (a), $2x10^{-5}$ mbar (b) and $2x10^{-7}$ mbar (c).

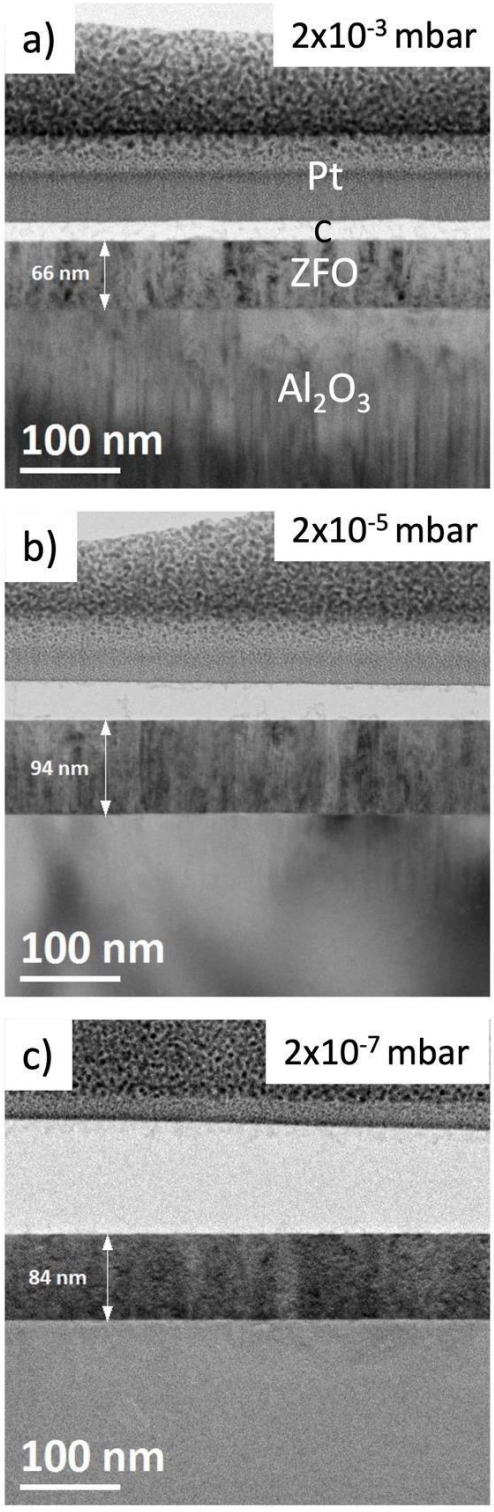

Fig. 4: Bright field TEM images of ZFO films grown by PLD on c-cut sapphire substrates at different oxygen partial pressures: (a) $2x10^{-3}$ mbar, (b) $2x10^{-5}$ mbar and (c) $2x10^{-7}$ mbar.

In each case, the electron beam direction is parallel to the [210] direction of the single crystalline Al_2O_3 substrate and thus perfectly parallel to the film/substrate junction. The film thicknesses are 66 nm, 94 nm and 84 nm, respectively. For the two highest pressure values (Figs 4a and 4b), the Bragg contrasts reveal a columnar growth of the films with sharp boundaries between the columns. Their width is a few tens of nanometers wide for $2x10^{-3}$ mbar and a little less for $2x10^{-5}$ mbar. The film grown with $2x10^{-7}$ mbar, presents less uniform contrasts with more diffuse boundaries between columns. Figure 5 shows the HREM images of the two former ZFO films depicting in each case the upper and the bottom parts of the films.

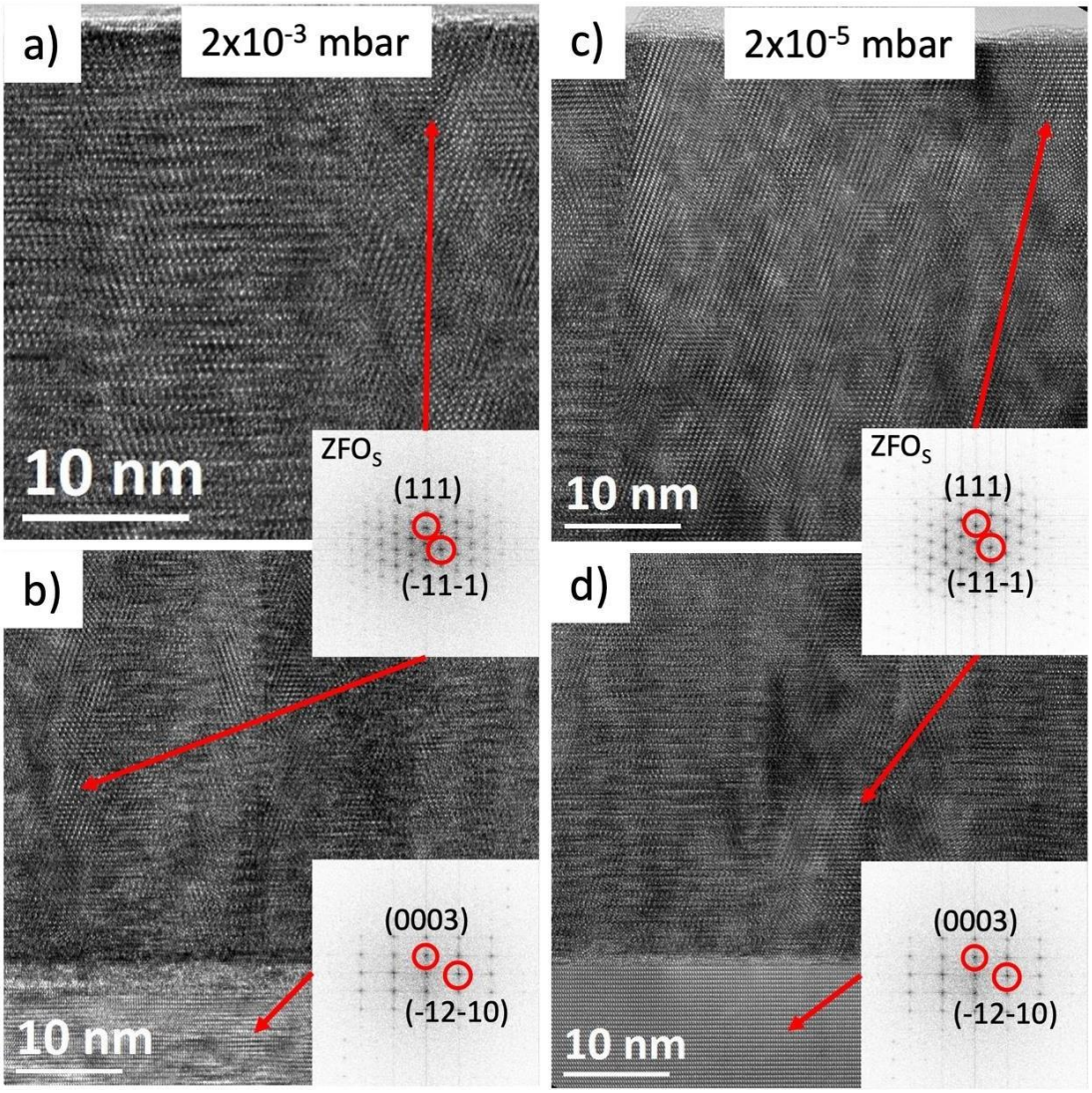

Fig. 5: HREM images of the top and bottom regions of the ZFO films grown under $2x10^{-3}$ mbar (a, b) and under $2x10^{-5}$ mbar (c, d). Insets are the FFTs of indicated regions of the c-cut sapphire substrate and the film.

In the insets, fast Fourier transforms (FFTs) are also reported and clearly indicate that both films are fully consistent with the magnetite spinel structure (FCC structure with a=0.839 nm) projected along a [101] direction. Note the (111) texture observed for both films, also highlighted in the XRD experiments (Fig. 2). The corresponding orientation relationships between the Al_2O_3 substrate and the ZFO_s film are the following:

(111) ZFO_s // (001) Al_2O_3 and [10-1] ZFO_s // [210] Al_2O_3

Figure 6 is a set of data of the ZFO film grown at $2x10^{-7}$ mbar. Figures 6a and 6b are HREM images of the top and bottom of the film, respectively.

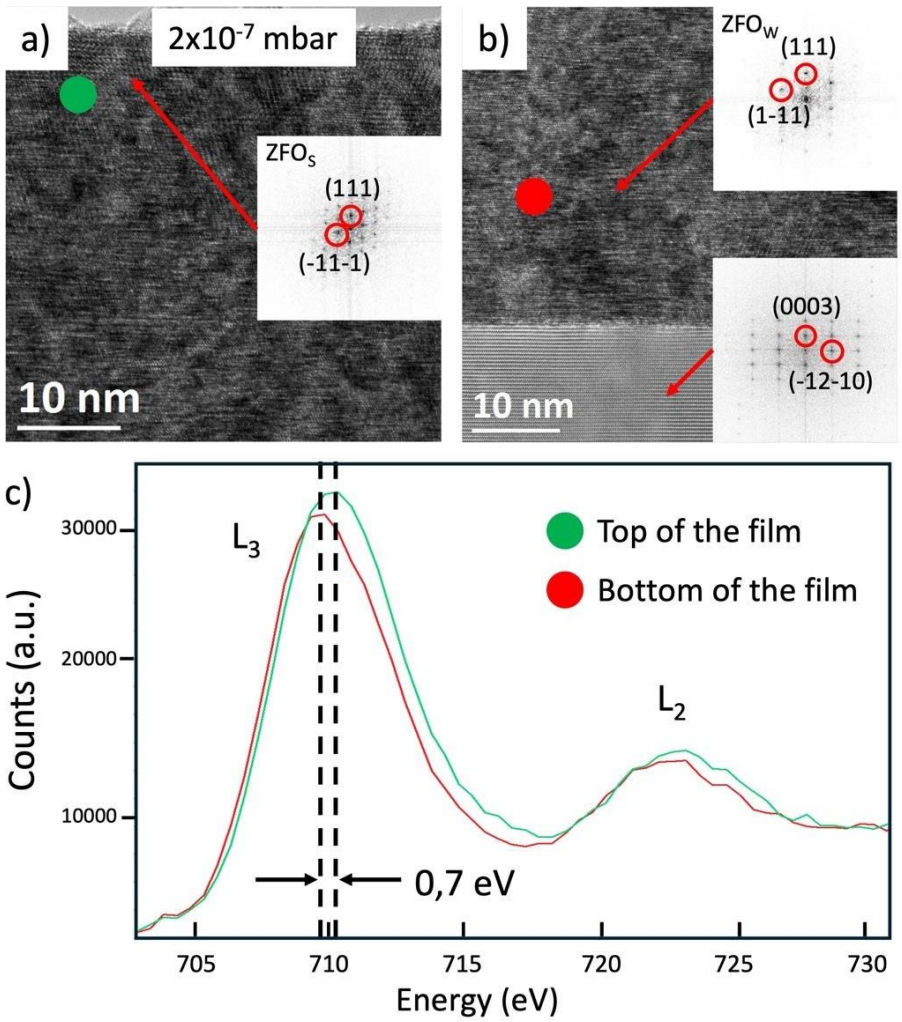

Fig. 6: HREM image of the top (a) and bottom (b) regions of the ZFO film grown with an oxygen partial pressure value of $2x10^{-7}$ mbar. Insets are the FFTs of the substrate and different parts of the film. The green and red spots are the pointed regions from which the EELS spectra shown in (c) were taken. The 0.7 eV shift of the L_3 threshold of iron is indicative of an evolution of its valence state in the upper part of the film.

The FFTs of different regions indicate that most part of the film is consistent with the wüstite structure (FCC structure with a=0.430 nm) oriented along a [10-1] direction revealing the (111) and (1-11) planes of ZFO_w with a d spacing of about 0.24 nm. The ZFO_w film is (111) textured as observed in the θ/2θ XRD patterns (Fig. 2) The corresponding orientation relationships between the Al_2O_3 substrate and ZFO_w film are those already observed by pole figure measurements and are as follows:

$$(111)\ ZFO_w\ //\ (001)\ Al_2O_3 \text{ and } [10\text{-}1]\ ZFO_w\ //\ [210]\ Al_2O_3$$

From Fig. 6, it can also be seen that the top region (about 15 nm thick) of the ZFO film consists of the magnetite structure. This thin upper layer of magnetite was not detected by asymmetric XRD because of its too low thickness value. Both wüstite and magnetite have a (111) texture and it is worth noticing that the epitaxial relationships between magnetite and wüstite are:

(111) ZFO_w // (111) ZFO_s and [10-1] ZFO_w // [-101] ZFO_s

To confirm the presence of both phases, EELS spectroscopy has been used to detect and compare the L_3 and L_2 iron thresholds for both regions. The corresponding spectra are shown in Fig. 6c and a clear shift of the L_3 peak (about 0.7 eV) towards higher energy values for the upper part of the film is observed. This is in agreement with an increase of the iron valence state from +II to a mixed valence state between +II and +III corresponding to the evolution of the film from Zn:FeO to Zn:Fe_3O_4 at the top of the film [45]. Note that a shift of 1.7 eV of the L_3 iron edge would have been observed for an iron valence state change from +II and +III.

Magnetic properties

The magnetic properties were studied through the magnetization M *versus* the external magnetic field μ_0H curves. Particular attention was paid to the ZFO film grown at RT under $2x10^{-7}$ mbar. Indeed, according to structural analyses by XRD and TEM, such a film is mainly constituted by the wüstite phase, since only the near surface region (about 15 nm thick) of the film reveals the presence of magnetite. The films obtained at higher pressures ($2x10^{-5}$ and $2x10^{-3}$ mbar) are constituted of magnetite phase without wüstite. The magnetic properties of magnetite-based ZFO films have already been studied in the past [46] while the origin of magnetism in non-stoichiometric FeO-based systems (powders, nanoparticles, thin films) is more difficult to explain. The M-H curves of the Zn:FeO film grown under $2x10^{-7}$ mbar have been recorded at 10K and 300K and are shown in Fig. 7.

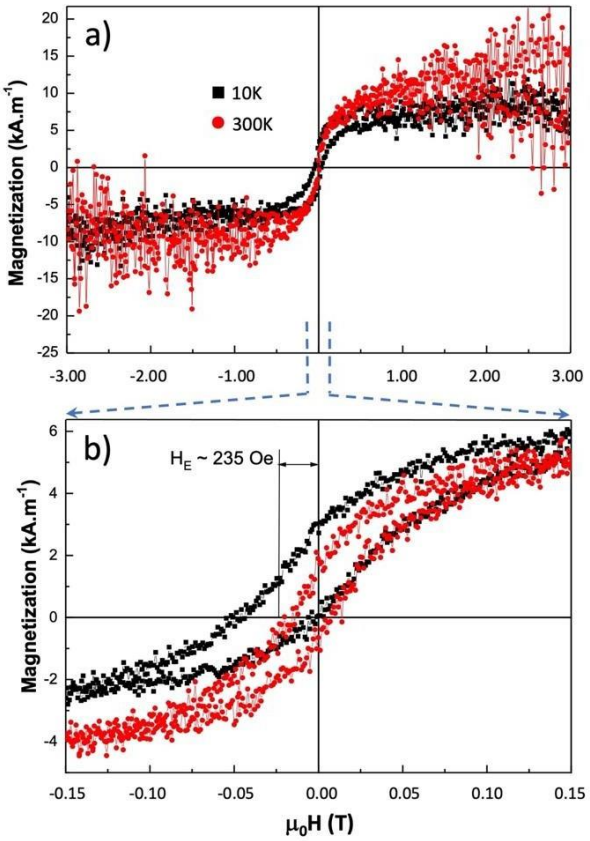

Fig. 7: M-H curves recorded for the wüstite-based ZFO films grown on c-cut sapphire substrate at RT under $2x10^{-7}$ mbar in the -3 to 3 T range (a) and in the low field region (b).

Fig. 7a represents the magnetization observed for applied magnetic fields in the -3 to 3 T range and Fig 7b, the M-H curve in the region of low fields. The hysteresis loops observed in Fig 7a is indicative of a ferrimagnetic behavior with non-zero coercivities and remanence magnetizations. This could be surprising since bulk wüstite is supposed to be antiferromagnetic with a Neel temperature of 198K [47] and to show a weak magnetic response. This ferrimagnetism has already been observed previously in non-stoichiometric $Fe_{1-x}O$ films grown by magnetron sputtering [48, 49] and its origin has been interpreted by the spinel-type defect clusters due to the presence of Fe^{3+} ions in the wüstite crystallographic network. This explanation is based on the theoretical study of Catlow and Fender [50] on the basic cluster formed by one tetrahedral Fe^{3+} ion and four cation vacancies in the cation-deficient wüstite FCC structure. Following the same approach, Gheisari *et al*. [51] explained the observed magnetization in wüstite nanoparticles by the presence of Fe_3O_4 spinel-like phase embedded in a stoichiometric FeO matrix. The chemical formula of the ZFO film grown under $2x10^{-7}$ mbar is $Zn_{0.21}Fe_{0.67}O_1$ which corresponds to the O/Fe = 1.17 (Table I). Assuming that this film is constituted by pure wüstite, the detailed formulae of a non-stoichiometric wüstite may be written: $Fe^{2+}_{(1-3x)}\ Fe^{3+}_{2x}\ \square_x\ O_1$, "x" being the proportion of cationic vacancies. It comes x=0.145 and consequently leads to the assumption of the presence of a high content of Fe^{3+} (29%) that explains the observed low ferrimagnetism.

The saturation magnetization Ms is low (8 $kA.m^{-1}$ and 10 $kA.m^{-1}$ at 300K and 10K, respectively) and much weaker than those measured for spinel-based ZFO films (500-600 $kA.m^{-1}$ depending on the crystalline state and the orientation of the ZFO films [46]). The hysteresis loops recorded at 10K are broader and shifted along the field axis toward the negative field, which indicates an exchange bias effect already reported for wüstite-based compound [52, 53]. The value of the exchange bias field H_E at 10K is around 235 Oe (0.0235 T) (Fig. 7b). This exchange bias is related to the ferromagnet-antiferromagnet interactions in our Zn:FeO films characterized by the presence of Fe^{3+} in the Fe^{2+} deficient wüstite phase, in addition to the presence of the thin layer of magnetite at the top of the film.

Discussion

The experimental results presented above highlight that the oxygen pressure during the growth allows obtaining epitaxial ZFO on c-cut substrate at RT. At high pressures, greater than $2x10^{-3}$ mbar, the films are amorphous with a chemical composition in agreement with the Fe_2O_3 phase. At intermediate $2x10^{-3}$ mbar and $2x10^{-5}$ mbar pressures, the ZFO films are crystallized and constituted by the Zn:Fe_3O_4spinel phase which is (111) oriented with well-defined epitaxial relationships with the (001) sapphire basal plane. More interestingly, the film grown under residual vacuum ($2x10^{-7}$ mbar) mainly consists of the Zn:FeO wüstite phase, the presence of spinel phase being detected only at the top of the films (about 15 nm thick over a 84 nm total film thickness). The presence of Fe^{3+} in such a film due to the presence of magnetite and/or cationic vacancies in the wüstite phase is also confirmed by the magnetic measurements. Nevertheless, it should be noted that the growth at RT of wüstite-based ZFO on c-cut sapphire is possible but complete removal of the spinel phase at the top surface of the film remains a challenge.

The oxygen pressure in the ablation chamber which ultimately plays a key role on both the oxygen content and crystalline structure of the ZFO films, influences the temporal and spatial distributions in the plasma plume of the species related to Zn, Fe and O which are emitted by the target after each laser pulse. The different phases and their crystalline state can be therefore explained following this way. The kinetic energy of the species emitted by the ZFO

target at each laser pulse is high (about 50 to 100 eV) [19] and could explain the preferential formation of a phase with low oxygen content (i.e. wüstite) in the film. In the case of residual vacuum (2 10^{-7} mbar), the O, Zn and Fe species will not interact with any gas and will thus preserve their initial kinetic energy [20, 54-56]. The velocity of the oxygen atoms coming from the target will be higher than that of the Fe and Zn atoms due to the difference in their atomic weights. It follows thus that a large part of the oxygen atoms coming from the oxide target, will arrive at the substrate surface before the Fe and Zn species, and thus will not participate in the film growth [57]. As a result, when the Zn and Fe atoms impact the substrate later, there are less oxygen atoms which leads to the preferential formation of the wüstite phase. In addition, the Zn and Fe species have preserved their high kinetic energy, and therefore have a high surface mobility allowing an easy crystallization of the film on the substrate. The epitaxial growth of the wüstite-based film is thus due to the high kinetic energy of these species.

In the intermediate situation between $2x10^{-5}$ and $2x10^{-3}$ mbar, the species coming from the target keep a significant part of their initial kinetic energy [56]. Indeed, even if their kinetic energy is slightly reduced by interaction with the oxygen introduced in the ablation chamber, sufficient surface mobility is preserved which allows the growth of crystallized and epitaxial film on the substrate. However, compared to the case of residual vacuum, the concentration of oxygenated species on the substrate surface being higher at these pressures, the formation of a more oxidized phase (i.e the spinel phase) can occur preferentially at the metastable wüstite phase.

For the films grown at higher pressures ($2x10^{-2}$ mbar), the species emitted by the laser pulse interact with oxygen atoms or molecules present in high concentration in the PLD chamber, as it has been reported elsewhere [57]. Consequently, all the emitted species will lose their kinetic energy during their movement towards the substrate, due to the numerous interactions in the plasma plume with oxygen species. Therefore, the Zn, Fe and O species will arrive simultaneously on the substrate with a low energy that excludes the formation of a crystalline film. An amorphous film will then be formed in these conditions, as it has been observed at this oxygen pressure.

The epitaxial relationships between the c-cut sapphire substrate and the wüstite ZFO_W film or the spinel ZFO_S film grown at RT are the same as those observed for ZFO films obtained on this substrate at elevated temperature (500°C) [58]. This relationship corresponds to a 30° rotation of the hexagons of the (111) ZFO (wüstite or spinel) on the hexagons of the (00l) sapphire planes. Classically, this epitaxial relationship is commonly due to the steps and terraces present at the surface of the sapphire substrate [12]. Such a treatment leads to an epitaxial film presenting steps and terraces at the surface of the film as shown by AFM measurements [12]. This type of epitaxial growth corresponds to the so-called graphoepitaxy [58]. In our case, the substrates were not heat-treated, but the AFM images (Fig. 1a) shows the presence of less defined steps than those obtained by thermal treatment (Fig. 1b), and the AFM image of the ZFO wüstite based film does not show steps and terraces (Fig. 1c). This result is drastically different from those reporting the presence of steps and terraces on film grown on heat-treated substrate [12]. A possible interpretation explaining the epitaxy of ZFO film on (00l) sapphire substrate without steps would be that the (00l) Al_2O_3 and the (111) ZFO planes are polar (planes containing either cations or anions). In this case, the epitaxy between the film and the substrate is based on the electrostatic interaction between the polar planes of ZFO and Al_2O_3. This epitaxy is very similar to the "quasi van der Waals epitaxy" in which there is little or no chemical bonding between the atoms of the film and substrate [59, 60].

Conclusions

We have grown successfully about 100 nm thick ZFO films by PLD on c-cut sapphire at RT under different oxygen pressures. At high pressure (greater than $2x10^{-3}$ mbar) amorphous films are obtained with a stoichiometry close to that of Fe_2O_3. For pressures between 2.10^{-3} and 2.10^{-5} mbar, films made of ZFO spinel (ZFO_s) are epitaxially grown on the c-cut sapphire substrate. The orientation relationships with the substrate are those commonly observed for ZFO films: they are the result of a 30° rotation of the hexagons of the (111) ZFO_S on the hexagons of the (00l) sapphire planes. Under vacuum limit ($2x10^{-7}$ mbar) a wüstite-based ZFO films (ZFO_w) can be obtained at RT even though the wüstite phase is not thermodynamically stable at RT. Well-defined epitaxial relationships between the ZFO_w film and the c-cut sapphire were demonstrated and the presence of magnetite in the upper part (around 15 nm thick) was highlighted by TEM experiments. The magnetic properties of the ZFO_w film reveal a ferromagnetic behavior explained by the presence of Fe^{3+} ions in the wüstite phase. The saturation magnetization values are relatively low (between 8 and 10 $kA.m^{-1}$ at 300K and 10K, respectively) and the exchange bias field value at 10K is around 235 Oe. This result comes from ferromagnet-antiferromagnet interactions in the film due to the presence of Fe^{3+} ions in the wüstite film and/or the presence of the thin layer of magnetite at the top of the film. Finally, the formations of the spinel or wüstite phases can be explained qualitatively by the different kinetic energies of the species emitted by the target in the plasma plume and the concentration of oxygenated species on the substrate surface with respect to the value of oxygen pressure.

Acknowledgements

XP is grateful to the ANR (Agence Nationale de la Recherche) organisation and the Normandie Region for their financial support in the acquisition of the EELS spectrometer and the FIB setup (ANR-11-EQPX-0020). He also thanks Franck LEMARIE for the preparation of the TEM samples. All the results reported in this manuscript fall within the scope of the research foundation IRMA (FR 3095). Pole figure measurements were performed on Osirix platform (ScanMAT, UAR 2025 University of Rennes-CNRS), which received a financial support from the European Union through the European Regional Development Fund (ERDF), the Département d'Ille et Vilaine, Rennes Métropole and Région Bretagne (2015-2020 CPER project SCANMAT).

References

1- D.P. Norton, *Synthesis and properties of epitaxial electronic oxide thin film materials*, Mat. Sci. Eng. R 43, 139 (2004)

2- J. Narayan, *Recent progress in film epitaxy across the misfit scale*, Acta Mater. 61, 2703 (2013)

3- A. Roemer, E. Millon, B. Vincent, A. Boudrioua, O. Pons-Y-Moll, R.M. Defourneau, W. Seiler, *Epitaxial $PbTiO_3$ thin films grown on (100) MgO by pulsed-laser deposition for optical waveguiding properties*, J. Appl. Phys. 95, 304 (2004).

4- S. Tricot, M. Nistor, E. Millon, C. Boulmer-Leborgne, N.B. Mandache, J. Perrière, W. Seiler, *Epitaxial ZnO thin films grown by pulsed electron beam deposition*, Surf. Sci. 604, 2024 (2010)

5- D. Rasic, R. Sachan, M.F. Chisholm, J. Prater, J. Narayan, *Room temperature growth of epitaxial titanium nitride by pulsed-laser deposition*, Crystal Growth & Design 17, 6634 (2017)

6- T. Kiyomura, M. Gomi, *Structural and magnetic properties of spinel ferrite epitaxial films pulsed-laser-deposited at low temperature*, Jpn. J. Appl. Phys. 40, 118 (2000)

7- V. Craciun, J. Perriere, N. Bassim, R.K. Singh, D. Craciun, J. Spear, *Low temperature growth of epitaxial ZnO films on (001) sapphire by ultraviolet-assisted pulsed laser deposition*, Appl. Phys. A 69, S531 (1999)

8- M. Yoshimoto, K. Shimozono, T. Maeda, T. Onishi, M. Kumagai, T. Chikyow, O. Ishiyama, M. Shinohara, H. Koinuma, *Room-temperature epitaxial growth of CeO_2 thin films on Si (111) substrates for fabrication of sharp oxide/silicon interface,* Jpn. J. Appl. Phys. 34, L688 (1995)

9- T. Onishi, M. Yoshimoto, G.H. Lee, T. Maeda, H. Koinuma, *Unit cell layer-by-layer heteroepitaxy of BaO thin films at temperatures a low as 20°C,* J. vac. Sci. Technol. A 209, 2769 (1997)

10- Y.T. Ho, K.S. Chang, K.C. Liu, L.Z. Hsieh, M.H. Liang, *Room temperature epitaxial growth of (001) CeO_2 on (001) $LaAlO_3$ by pulsed laser deposition*, Cryst. Res. Technol. 48, 308-313 (2013)

11- K. Shimomoto, A. Kobayashi, K. Mitamura, K. Ueno, J. Ohta, M. Oshima, H. Fujika, *Characteristics of m-plane InN films grown on ZnO substrates at room temperature by pulsed laser deposition,* Jpn. J. Appl. Phys. 49, 080202 (2010)

12- A. Matsuda, R. Yamauchi, D. Shiojiri, G. Tan, S. Kaneko, M. Yoshimoto, *Room-temperature selective epitaxial growth of CoO (111) and Co_3O_4 (111) thin films with atomic steps by pulsed laser deposition,* Appl. Suf. Sci. 349, 78 (2015)

13- X.B. Liu, H.B. Lu, M. He, K.J. Jin, G.Z. Yang, *Room-temperature epitaxial growth of V_2O_3 films,* Sci. China-Phys. Mech. Astron. 57, 1866 (2014)

14- Y. Kakehi, S. Nakao, K. Satoh, T. Kusaka, *Room-temperature epitaxial growth of NiO (111) thin films by pulsed laser deposition,* J. Cryst. Growth 237-239, 591 (2002)

15- T. Kiyomura, M. Gomi, *Room-temperature epitaxial growth of Ni-Zn ferrite thin films by pulsed laser deposition in high vacuum,* Jpn. J. Appl. Phys. 36, L1000 (1997)

16- A. Matsuda, S. Akiba, M. Kasahara, T. Watanabe, Y. Akita, Y. Kitamoto, T. Tojo, H. Kawaji, T. Atake, K. Koyama, M. Yoshimoto, *Fabrication of ferromagnetic Ni epitaxial thin film by way of hydrogen reduction of NiO,* Thin Solid Films 516, 3873(2008)

17- M. Yoshimoto, T. Maeda, T. Ohnishi, H. Koinuma, O. Ishiyama, M. Shinohara, M. Kubo, R. Miura, A. Piyamoto, *Atomic-scale formation of ultrasmooth surfaces on sapphire substrates for high-quality thin film fabrication,* Appl. Phys. Lett. 67, 2615 (1995)

18- M. Yoshimoto, A. Sasaki, S. Akiba, *Nanoscale epitaxial growth control of oxide thin films by laser molecular beam epitaxy – towards oxide nanoelectronics,* Sci. Technol. Adv. Mater. 5, 527 (2004)

19- J.T. Gudmundson, A. Anders, A. von Kendell, *Foundations of physical vapor deposition with plasma assistance*, Plasma Sources Sci. Technol. 31, 083001 (2022).

20- V. Trtik, A. Perez, J. Navarro, C. Ferrater, F. Sanchez, M. Varela, *Influence of laser-ablation plume dynamics on the room-temperature epitaxial growth of CeO_2 on silicon,* Appl. Phys. A 69, S815 (1999)

21- M. Yoshimoto, R. Yamauchi, D. Shiojiri, G. Tan, S. Kaneko, A. Matsuda, *Room-temperature synthesis of epitaxial oxide thin films for development of unequilibrium structure and novel functionalization,* J. Ceram. Soc Japan 121, 1 (2013)

22- Y.K. Kim, M. Oliveria, *Magnetic properties of reactively sputtered Fe1-x O and Fe3O4 thin films,* J. Appl. Phys. 75, 431 (1994)

23- Y. Peng, C. Park, D.E. Laughlin, *Fe3O4 thin films sputter deposited from iron oxide targets,* J. Appl. Phys. 93, 7957 (2003)

24- S. Tiwari, R. Prakash, R. J. Choudhary, D. M. Phase, *Oriented growth of Fe3O4 thin film on crystalline and amorphous substrates by pulsed laser deposition* J. Phys. D: Appl. Phys. 40, 4943 (2007)

25- X. Liu, H. Lu, M. He, L. Wang, H. Shi, K. Jin, C. Wanh, G. Yang., *Room-Temperature Layer-by-Layer Epitaxial Growth and Characteristics of Fe3O4 Ultrathin Films,* J. Phys. Appl. Phys. 47, 105004 (2014)

26- C-E Bejjit, V. Rogé, C. Cachoncinlle, C. Hebert, J. Perrière, E. Briand, E. Millon, *Iron oxide thin films grown on (00l) sapphire substrate by pulsed-laser deposition,* Thin Solid Films 745, 139101 (2022).

27- V. Demange, X. Portier, S. Ollivier, M. Pasturel, T. Roisnel, M. Guilloux-Viry, C. Hebert, M. Nistor, C. Cachoncinlle, E. Millon, J. Perrière, *Room-temperature epitaxial growth of Zn-doped iron oxide films on c-, a- , and r-cut sapphire substrates,* Crystal Growth & Design 23, 8534 (2023)

28- Y. Thimont, J. Clatot, M. Nistor, C. Labrugere, A. Rougier, *From ZnF_2 to ZnO films using pulsed-laser deposition: Optical and electrical properties,* Solar Energy Materials and Solar Cells 107, 136-141 (2012)

29- P. Atanasov, R.I. Tomov, J. Perrière, R. Eason, N. Vainos, A. Klimi, A. Zherikhin, E. Millon, *Growth of Nd:potassium gadolinium tungstate thin-film waveguides by pulsed laser deposition,* Appl. Phys. Lett., 76, 2490 (2000)

30- J. Clatot, M. Nistor, A. Rougier, *Influence of Si concentration on electrical and optical properties of room temperature ZnO:Si thin films,* Thin Solid Films 531, 197 (2013).

31- C. Marechal, E. Lacaze, W. Seiler, J. Perrière, *Growth mechanisms of laser deposited BiSrCaCuO films on MgO substrates,* Physica C 294, 23 (1998)

32- E. Le Boulbar, E. Millon, J. Mathias, C. Boulmer-Leborgne, M. Nistor, F. Gherendi, N. Sbaï, JB. Quoirin, *Pure and Nb-doped TiO1.5 films grown by pulsed-laser deposition for transparent p-n homojunctions*, Appl. Surf. Sci. 257, 5380 (2011).

33- N. Chaoui, E. Millon, J.F. Muller, P. Ecker, W. Bieck, H.N. Migeon, *On the role of ambient oxygen in the formation of lead titanate pulsed laser deposition thin films*, Appl. Surf. Sci. 138, 256 (1999)

34- N. Chaoui, E. Millon, J.F. Muller, P. Ecker, W. Bieck, H.N. Migeon, *Perovskite lead titanate PLD thin films: study of oxygen incorporation by O^{18} tracing techniques*, Mat. Chem. Phys. 59, 114 (1999)

35- M. Nistor, A. Petitmangin, C. Hebert, W. Seiler, *Nanocomposite oxide thin films grown by pulsed energy beam deposition*, Appl. Surf. Sci. 257, 5337 (2011).

36- R. Yamauchi, Y. Hamasaki, T. Shibuya, A. Saito, N. Tsuchimine, K. Koyama, A.Matsuda, M. Yoshimoto, *Layer matching epitaxy of NiO thin films on atomically stepped sapphire (0001) substrates*, Sci. Rep. 5, 14385 (2015)

37- Y. Fuji, M. Hara, H. Yuasa, S. Murakami, and H. Fukuzawa, *Enhancement of magnetoresistance by ultra-thin Zn wüstite layer*, Appl. Phys. Lett. 99, 132103 (2011)

38- S.G. Bhat and P. S. Anil Kumar, *Investigation on the origin of exchange bias in epitaxial, oriented and polycrystalline Fe3O4 thin films*, AIP Advances 5, 117123-1 (2015)

39- S. Moll, S.-U. Weber, K.-D. Becker, W. Mader, *Solid Solutions in the System Fe1–xO/ZnO at Low Oxygen Partial Pressure*, Z. Anorg. Allg. Chem. 636, 1880 (2010)

40- J. Perrière, C. Hebert, M. Nistor, E. Millon, J.J. Ganem, N. Jedrecy, *$Zn_{1-x}Fe_xO$ films: from transparent Fe-diluted ZnO wurtzite to magnetic Zn diluted Fe_3O_4 spinel*, J. Mat. Chem. 3, 11239 (2015)

41- P. Pant, J.D. Budai, R. Aggarwal, R. Narayan, J. Narayan, *Thin film epitaxy and structure property correlations for non-colar ZnO films*, Acta Mater. 57, 4426 (2009)

42- J. Narayan, K. Dovidenko, A.K. Sharma, S. Oktyabrsky, *Defects and interfaces in epitaxial ZnO/α-Al_2O_3 and AlN/ZnO/α-Al_2O_3 heterostructures*, J. Appl. Phys. 84, 2597 (1998)

43- W. Seiler, M. Nistor, C. Hebert, J. Perrière, *Epitaxial undoped indium oxide thin films : Structural and physical properties*, Solar En. Mat. Solar Cells 116, 34 (2013)

44- M. Nistor, E. Millon, C. Cachoncinlle, W. Seiler, N. Jedrecy, C. Hebert, J. Perrière, *Transparent conductive Nd-doped ZnO thin films*, J. Phys. D 48, 195103 (2015)

45- C. Colliex, T. Manoubi, C. Ortiz, Electron-energy-loss-spectroscopy near-edge fine-structures in the iron-oxygen system, Phys. Rev. B 44, 11402 (1991)

46- N. Jedrecy, C. Hebert, J. Perriere, M. Nistor, E. Millon, *Magnetic and magneto-transport properties of ZnxFe3−xO4−y thin films*, J. Appl. Phys. 116, 213903 (2014)

47- R.M. Cornell, U. Schwertman, *The iron oxides : structure, properties, occurrences, and uses*, VCH, Weinheim, 1996. ISBN 3-527-28576-8

48- D.V. Dimitrov, K. Unruh, G.C. Hadjipanayis, V. Papafthymiou, A. Simopoulos, *Defect clusters in Fe1-xO and their ferrimagnetic properties*, J. Appl. Phys. 87, 7022 (2000)

49- Y. K. Kim and M. Olivetia, *Magnetic properties of reactively sputtered $Fe_{1-x}0$ and Fe&, thin films*, J. Appl. Phys. 75, 431 (1994)

50- C.R.A. Catlow, B.E.F. Fender, *Calculations of defect clustering in Fe1-xO*, J. Phys. C, Solid State Phys. 8, 3267 (1975)

51- M. Gheisari, M. Mozaffari, M. Acet, J. Amighian, *Preparation and investigation of magnetic properties of wüstite nanoparticles*, J. Magnetism and Magnetic Materials 320, 2618 (2008)

52- M. Gheisari, M. Mozaffari, M. Niyaifar, J. Amighian, *Observation of small exchange bias in defect wüstite ($Fe_{0.93}O$)*, J. Superconductivity and novel magnetism 26, 237 (2013)

53- P.V.M. Shameen, L. Mekala, S Kumar, *Structural and magnetic properties of non-stoichiometric $Fe_{1-x}O$*, AIP Conf. Proc. 1942, 080077 (2018)

54- S. Amoruso, B. Toftmann, J. Schou, *Thermalization of a UV laser ablation plume in a background gas: from a directed to a diffusion like flow*, Phys. Rev. E 69, 056403 (2004)

55- S. Amoruso, B. Toftmann, J. Schou, R. Velotta, X. Wang, *Diagnostics of laser ablated plasma plumes*, Thin Solid Films 453, 562-572 (2003)

56- T. Wijnands, E.P. Houwman, G. Koster, G. Rijnders, M. Huijben, *Numerical modeling of the plasma plume propagation and oxidation during pulsed laser deposition of complex oxide thin films*, Phys. Rev. Mat. 4, 103803 (2020).

57- X. Portier, C. Hebert, E. Briand, J. Perrière, E. Millon, C. Cachoncinlle, M. Nistor, N. Jedrecy, *Microstructure of nanocomposite wurtzite-spinel (Fe:ZnO)-(Zn:Fe_3O_4) epitaxial films*, Mat. Chem. Phys. 229, 130 (2019)

58- P.B. Mozhaev, J.E. Mozhaeva, A.V. Khoryushin, J.B. Hansen, C.S. Jacobsen, I.K. Bdikin, I.M. Kotelyanskii, V.A. Luzanov, *Three dimensional graphoepitaxial growth of oxide films by pulsed laser deposition*, Phys. Rev. Mater. 2, 103401 (2018)

59- Y-H. Chu, *« Van der Waals oxide heteroepitaxy »*, NPJ Quantum Materials 2, 67 (2017)

60- S. Ke, J. Xie, C. Chen, P. Lin, X. Zeng, L. Shu, L. Fei, Y. Wang, M. Ye, D. Wang, *Van der Waals epitaxy of Al-doped ZnO film on mica as a flexible transparent heater with ultrafast thermal response*, Appl. Phys. Lett. 112, 031905 (2018)